Published in final edited form as:

Biomacromolecules. 2017 February 13; 18(2): 562–567. doi:10.1021/acs.biomac.6b01715.

Implantable Tin Porphyrin-PEG Hydrogels with pH-responsive Fluorescence

Haoyuan Huang[a], **Saurabh Chauhan**[b], **Jumin Geng**[a], **Yiru Qin**[a], **David F. Watson**[b], and **Jonathan F. Lovell**[a]

[a]Department of Biomedical Engineering, University at Buffalo, State University of New York, Buffalo, NY, USA

[b]Department of Chemistry, University at Buffalo, State University of New York, Buffalo, NY, USA

Abstract

Tetracarboxy porphyrins can be polymerized with polyethylene glycol (PEG) diamines to generate hydrogels with intense, near infrared, and transdermal fluorescence following subcutaneous implantation. Here, we show that the high density porphyrins of the pre-formed polymer can be chelated with tin via simple incubation. Tin porphyrin hydrogels exhibited increasing emission intensities, ratios, and lifetimes from pH 1 to 10. Tin porphyrin hydrogel emission was strongly reversible and pH responsiveness was observed in the physiological range between pH 6 to 8. pH sensitive emission was detected via non-invasive transdermal fluorescence imaging in vivo following subcutaneous implantation in mice.

Table of Contents

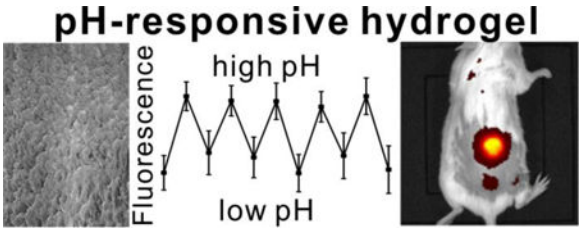

Keywords

Porphyrin; Hydrogel; pH Biosensor; Fluorescence

Introduction

Hydrogels are three dimensional, hydrophilic polymers with a range of potential applications in tissue engineering, drug delivery and biosensing.[1] Frequently, hydrogel biosensors aim to provide a fluorescent output that responds to the presence of chemicals based on changes induced by hydrogel swelling, or by interaction of analytes with encapsulated dyes.[2] Numerous detection dyes have been immobilized in hydrogel scaffolds for in vivo monitoring of oxygen [3, 4], glucose [5–7], pH [8] and even cancer cells [9].

The pH of physiological fluid plays a critical role in biochemical function. Different body fluids have different pH levels [10]. Metabolic disorders [11] and brain tissue damages [12] have been proposed to be diagnosed by unusual pH. Abnormal intracellular pH has been associated with inappropriate cellular functions, which may be implicated to cancers[13] and Alzheimer's disease[14].

A diversity of molecules can report changes in pH via changes in optical absorption or fluorescence.[15]. Several fluorescent dyes have been reported as pH sensitive optical sensors, such as fluorescein[16, 17], carbazolyl-pyridinyl conjugate[18], carbon nanodots[19], IR or NIR BODIPY dyes [20], and silver nanoclusters[21].

Porphyrins and related molecules have useful characteristics for theranostic applications [22–25]. Polyethylene glycol (PEG) is known to modulate in vivo behavior of tetrapyrroles. [26, 27] We previously found that hydrogels could be formed with PEG diamines crosslinked with meso-tetra(4-carboxyphenyl)porphine (mTCPP) to enable transdermal fluorescence guided hydrogel tracking and surgical resection.[28] These bright hydrogels have extreme dye density (5 mM) with minimal self-quenching, due the three dimensional spatial confinement within a PEG mesh. By using the Pd version of mTCPP (Pd mTCPP), the resulting hydrogels had luminescence that decreased at higher oxygen concentrations, thereby creating a biosensor that could be implanted in mice and detect subcutaneous oxygen changes via transdermal phosphorescence imaging.[3]

Tin porphyrins have been shown in many circumstances to exhibit pH dependent optical properties. $SnCl_2$-tetraphenyl porphyrin (similar to the free base porphyrin monomer used in porphyrin-PEG hydrogels) has a pH dependent fluorescence emission that increases from pH 2 to pH 10.[29] $SnCl_2$-tetraphenyl porphyrin membranes demonstrated pH responsiveness. [30] Ionic $SnCl_2$ porphyrins have also been shown to have fluorescence properties that depend on pH.[31] The fluorescence of tetrapyridyl and tetramethylpyridinium tin porphyrins in solution depends on pH.[32] Based on these observations, we hypothesized that tin could be chelated into the porphyrin-PEG hydrogels to confer pH sensitive fluorescence for potential uses in biomedical applications.

Materials and methods

Materials

Unless otherwise specified, reagents were obtained from Sigma. Meso-tetra(4-carboxyphenyl) porphyrin (mTCPP) was obtained from Frontier Scientific. Polyethylene glycol (PEG) 6000 was obtained from Rapp Polymere. O-(Benzotriazol-1-yl)-N,N,N',N'-tetramethyluronium hexafluorophosphate (HBTU) was obtained from Advanced Chem Tech. N,N-Diisopropylethylamine (DIPEA) was obtained from TCI. Tin(II) chloride dihydrate was obtained from Alfa Aesar. ICR mice were ordered from Harlan Laboratories Inc. Reli Black Nylon-monofilament Sutures (cat # N931) were obtained from MYCO Medical.

mTCPP-PEG hydrogel synthesis

mTCPP, PEG-diamine and HBTU were dissolved separately in dimethylformamide (DMF) to make 15 mM, 30 mM and 60 mM stock solutions. Equal volumes of mTCPP and HBTU stock solutions were mixed, and 26.6 μL of this solution was added to each well of a polypropylene 96-well plate. After adding 2 μL of 10% DIPEA in DMF, 13.4 μL of PEG-6K solution was added. The total molar ratio of reactants were mTCPP:PEG-6K:HBTU=1:2:4, which matches their stoichiometric ratio of the reactive groups. After 30 minutes, excess DMF was added to stop the polymerization and to remove unincorporated reactants.

Synthesis of $SnCl_2$-meso-tetra(4-carboxyphenyl)porphine (Sn-mTCPP)

The synthetic procedure was based on that reported by Manke et al.[33] Briefly, 200 mg of mTCPP (0.25 mM) was mixed with 113 mg $SnCl_2 \cdot 2H_2O$ (0.50 mM) under nitrogen. 5 mL anhydrous pyridine was added to the system and the solution was heated to refluxed for 2 h in the dark. After cooling, 30 mL diethylether was added and stirred at 4 °C in the dark for 12 h. Purple precipitates were collected by filtration and washed with ether, CH_2Cl_2, water and ether again. The final product was dried in the vacuo. Yield was 72.1% (178.6 mg). MALDI-MS: m/z=908 ($[M-2Cl]^+$), 943 ($[M-Cl]^+$). ^{1}H-NMR (300 MHz, DMSO-d6): d = 13.30 (s, 4H, O-*H*), 9.27 (s, 8H, pyrrole-*H*), 8.44–8.39 (d, ^3J = 16H, ortho-*H* and meta-*H*) ppm, as shown in Figure S1.

Chelation of tin into preformed mTCPP-PEG hydrogels

120 mg of $SnCl_2 \cdot 2H_2O$ was mixed with 24 hydrogel pucks in anhydrous pyridine. The reaction proceeded for 3 h under nitrogen. Then hydrogels were then washed in DMF and water to remove pyridine and unreacted $SnCl_2$.

To study the kinetics of tin chelation into the hydrogel, a standard curve was made with different ratios of $SnCl_2$mTCPP:mTCPP ranging from 0–100%. Then the mixture was polymerized to hydrogels as the same procedure as mTCPP hydrogel synthesis. After the synthesis, fluorescent intensities of hydrogels were tested with TECAN Safire plate reader and the standard curve of fluorescent ratio at 600nm and 650nm to $SnCl_2$mTCPP ratio. The standard curve was shown as Figure S2 and R^2=0.99838. Then, mTCPP hydrogels were post chelated with $SnCl_2 \cdot 2H_2O$ and collected at 0, 5, 60, 120 and 180 min after the temperature reached 60 °C. Fluorescent spectra of the hydrogels were scanned and the ratios of fluorescent intensities of hydrogels at 600 nm and 650 nm were calculated and compared with the standard curve.

Reversible pH sensitivity of $SnCl_2$mTCPP hydrogels

$SnCl_2$mTCPP hydrogels were put in the well of 96-well plate and fluorescent intensities at 600 nm were tested with plate reader. Then 200 μL of different pH 100 mM sodium phosphate solution was added to the well and incubated for 5 min, then pH solutions were removed and fluorescent signals were tested again.

For testing pH sensitivity of hydrogels, they were put in 96-well plate and treated with acidic or basic pH 100 mM sodium phosphate solutions of indicated pH for 5 min alternately. Fluorescent intensities at 600 nm (for $SnCl_2$mTCPP hydrogels) or 650 nm (for 2H mTCPP)

were read by the plate reader and alternating acidic and basic pH solutions were added and fluorescent signals were read time after each incubation. Fetal bovine serum (FBS) was added to pH=4 and pH=10 100mM sodium phosphate solutions to make 10% FBS pH buffer. The reversible curve was tested with the same procedure as the experiments without FBS.

Fluorescent lifetime decay

Time resolved photoluminescence decay traces were obtained by a Becker and Hickl Tau-130 time correlated single photon counting (TCSPC) setup. The setup consisted of a vertically polarized pulsed diode laser (BDL 445 SMC) emitting monochromatic radiation at 445 nm at 20 MHz repetition rate. The hydrogel samples were placed on a glass slide inside a four side quartz cuvette and the cuvette was filled with corresponding buffer solution in which hydrogel was kept in. The emission from the hydrogel samples was collected at 90 degrees from excitation beam and focused into a polychromator coupled to a 16 channel photomultiplier tube (PML 16C). Each channel corresponded to 12.5 nm in the wavelength regime. All measurements were taken at magic-angle conditions by putting a polarizer in the emission channel at 54.7 degrees to the polarization of the excitation beam. A 470 nm longpass filter was used to avoid scattering of excitation beam from the glass film. A neutral density filter was placed in the excitation pathway to control the intensity of the excitation pulses in such a way that the probability of detection of a photon per excitation pulse was less than 0.01. The decay traces for each sample were collected for 300 s over 4096 time bins with a time resolution of 12.2 ps. Instrument response function (IRF) was acquired by collecting scattered light by silica LUDOX solution. At a laser gain of 20% and detector gain of 90%, the full width half maximum (FWHM) of IRF was approximately 220 ps. The collected decay traces were fitted by using Fluofit software by Picoquant.

TRPL decay traces were fitted by using multi-exponential reconvolution to equation 1:

$$I(t) = \int_{-\infty}^{t} IRF(t') \sum_{(i=1)}^{n} A_i exp\left(-\frac{t-t'}{\tau_i}\right) dt' \quad (1)$$

Where I(t) is the intensity of PL decay, IRF(t') is the instrument response function and Ai is the amplitude of the lifetime component τi. The decay profiles were fit with single or bi-exponential fits, whichever produced a good fit. The goodness of fit was evaluated by distribution of residuals (difference between raw and fit data) around zero and chi-square values. Single and bi-exponential fits with corresponding chi-square values for representative hydrogels are shown in supporting information. Chi-square values between 0.9–1.2 were considered as good fits. Intensity weighted average lifetime values <τ> for corresponding decay profiles were calculated according to equation 2:

$$< \tau > = \frac{\sum A_i \tau_i^2}{\sum A_i \tau_i} \quad (2)$$

Animal experiments

Animal experiments were conducted in compliance with University at Buffalo Institutional Animal Care and Use Committee policy. To determine the control group through fluorescent intensity, 85%Cu/15%2H, 90%Cu/10%2H and 95%Cu/5%2H mTCPP hydrogels were put in 96-well plate with $SnCl_2$mTCPP hydrogels, and the fluorescent photos were tested with an IVIS imaging system with excitation at 640 nm and using the emission signal with the Cy5.5 filter. Mice were anesthetized with 2% (v/v) isoflurane in 100% oxygen carrier gas. Under deep anesthesia, two small incisions were made on the back of mice, then $SnCl_2$mTCPP hydrogels and 95% Cu-mTCPP/ 5% mTCPP hydrogels were implanted. The incisions were closed with sutures. Fluorescence images of hydrogels were acquired with an IVIS system with mice under isoflurane anesthesia. For pH sensitive tests, 200 μL of pH=4 and pH=10 100 mM sodium phosphate solutions were injected subcutaneously near the areas around hydrogels, and fluorescent photos were scanned 1h post injection.

Results and discussion

Synthesis and characterization of tin porphyrin-PEG hydrogels

Figure 1A shows the schematic of the synthesis of freebase (2H) mTCPP hydrogels and subsequent chelation with $SnCl_2$. 2H-mTCPP hydrogels consist of a highly crosslinked and high density porphyrin-PEG mesh. The polymerization of 2H-mTCPP and PEG was carried out in DMF with HBTU as the coupling condensation agent to form the polyamide. The reaction completed within seconds after adding DIPEA to initiate the reaction. The ratio of mTCPP:PEG:HBTU was 1:2:4, which corresponds to the equimolar ratios of functional groups of tetracarboxylic porphyrin, diamine PEG and the HBTU acid activator. The resulting hydrogels were washed with DMF to remove the unincorporated reactants.

2H-mTCPP hydrogels were then mixed with $SnCl_2$•$2H_2O$ to post chelate $SnCl_2$ to the center of 2H-mTCPP. The post chelation process took 3h at 60 °C in pyridine. After the reaction, hydrogels were washed in DMF and then with water several times to remove organic solvents and unreacted $SnCl_2$ (Figure 1A). The kinetics of the chelation process (Figure 1B) was examined by comparing the fluorescence ratios of the emission intensities at 600 nm and 650 nm of the reacted hydrogels a standard curve formed from hydrogels composed of defined ratios of tin and 2H porphyrins (Figure S2). As shown in Figure 1B, the chelation process reached a ~90% yield within 2 hours. The absorbance and fluorescent spectra of mTCPP hydrogel and $SnCl_2$mTCPP post chelated hydrogels are shown in Figure 1C and 1D, respectively. After tin chelation, the absorbance peak of hydrogels shifts subtly from 420 nm to 425 nm, and fluorescence emission blue shifts from 650 nm and 720 nm to 600 nm and 650 nm, resulting a narrower Stokes shift. Absorbance and fluorescence spectra of tin porphyrin hydrogels were the same whether tin was chelated into pre-formed hydrogels or whether tin-porphyrins were in the polymerization reaction (Figure S3). Post-chelating tin into preformed freebase hydrogels has the advantage that a single batch of porphyrin hydrogels can be used for multiple applications and post-chelation was the approach used for this work. Scanning electron microscopy of freeze-dried tin hydrogel is shown in Figure 1D, demonstrating a disordered but highly interconnected $SnCl_2$mTCPP-PEG environment.

pH-dependent emission of $SnCl_2$mTCPP hydrogel

Axial water molecules of tin (IV) porphyrins can lose protons to yield a hydroxide-coordinated metal compounds to create pH-responsive properties.[30] Tin-porphyrin-PEG-hydrogels exhibited pH responsive properties. As shown in Figure 2A, in low pH, fluorescent emission of the tin hydrogels reached the lowest levels. As pH increased towards neutral, fluorescence intensities at 600 nm emission increased. As pH increased even further to basic ange, the fluorescence increased to a higher level, almost 4 fold higher than at pH=1. The ratio of the hydrogel fluorescence at 600 nm and 650 nm offers a quantitative way to gauge pH (Figure 2B). Free base porphyrin hydrogels demonstrated some pH sensitivity (Figure S4), however this was only at very low pH (i.e., pH<3) with little physiological relevance. As shown in Figure 2C **and** Table S1 the average lifetime of tin hydrogels increased from (0.9±0.05) ns to (1.6±0.05) ns, consistent with steady-state emission enhancement as pH increased from 1 to 10.

Reversibility of pH Responsiveness

The pH reversibility of the hydrogels was assessed. As shown in Figure 3A and 3B, tin-porphyrin-PEG hydrogels exhibited strong fluorescence reversibility between pH=4 and pH=10 solutions, even following a week of storage. Such behavior was not observed at all in freebase porphyrin hydrogels lacking tin. The pH reversibility was also assessed in the presence of proteins, since these would be encountered in potential in vivo applications. Based on Figure 3C and 3D, the $SnCl_2$mTCPP hydrogels also possessed a similar reversible emission pattern when incubated with 10% fetal bovine serum in pH=4 and pH=10 solutions, while still no reversible pattern was exhibited for hydrogels lacking tin.

Next, tin-porphyrin-PEG hydrogels were assessed for pH responsiveness in more physiologically relevant, intermediate pH ranges. As shown in Figure 4A, fluorescent signals from hydrogels increased from acidic to basic conditions, and the fluorescence at the neutral condition (pH=7) formed the middle position of the curve. The opposite curve was also observed when pH lowered down from basic system to the acidic circumstance. Then the similar tests were processed with narrower pH range, as shown in Figure 4B and 4C, hydrogels demonstrated the similar reversibility under two pH pairs, pH=5 and 9, and pH=6 and 8, respectively. $SnCl_2$mTCPP hydrogels also demonstrated reversible emission with pH=6.5 and ph=7.4 PBS buffer (Figure 4D), demonstrating the potential for pH sensing in physiological relevant conditions. For example, the pH of the extracellular fluid will affect several cellular activation, and is known to influence the wound healing process.[34, 35] Therefore, a non-invasive and continuous sensor to monitor pH of subcutaneous extracellular fluid could conceivably help guide certain medical treatments.

In vivo pH sensitivity

We next assessed tin-porphyrin-PEG hydrogels for detection of pH in mice following subcutaneous implantation. Previously, when investigating Pd-porphyrin hydrogels with oxygen-responsive phosphorescence, we blended non-fluorescent copper mTCPP with freebase mtCPP to make an emission intensity matched control hydrogel.[3] In this manner, the two could be implanted simultaneously for ratiometric imaging since only Pd porphyrin hydrogels were oxygen responsive. To this same end, the fluorescence intensities of

hydrogels formed with varying ratios of copper and freebase porphyrins were assessed and compared to the $SnCl_2$mTCPP hydrogels. As shown in Figure 5A, 95:5 Cu:2H mTCPP hydrogels generated similar fluorescence intensity as $SnCl_2$mTCPP hydrogels. Thus 95:5 Cu-mTCPP: 2H-mTCPP hydrogels were co-implanted as a non-responsive companion hydrogel. The hydrogels were implanted subcutaneously on the dorsum of mice. Whole body fluorescence imaging easily detected the hydrogels through the skin of mice (Figure 5B). Unexpectedly, in vivo the Cu:2H companion hydrogel exhibited weaker emission relative to the tin-porphyrin-PEG one, but nevertheless could be used for ratiometric applications. Following injection of a pH=4 phosphate solution, the fluorescence of the tin hydrogels decreased, but the Cu:2H one remained constant (Figure 5B). For in vivo pH-responsivity, the changes in fluorescence intensities were demonstrated as the variations of the ratios of the tin to freebase hydrogels, pre- and post-injection with pH=4 and pH=10 100 mM sodium phosphate solutions. As shown in Figure 5C and Figure 5D, pH=4 phosphate solution decreased the emission of the tin hydrogel by about 20% while pH=10 solutions increased the intensity about 30%, which roughly matches in vitro the pH-responsive pattern.

Mice tolerated tin porphyrin hydrogel implantation and imaging without incident. Tin and tin alloys have been used in routine human life for thousands of years (e.g. in plates and mugs) and are generally safe, whereas organotin compounds containing C-Sn bonds (absent from the hydrogel) are toxic.[36] A tin-chelated chlorin, tin etiopurpurin, has been used clinically with intravenous injection for photodynamic therapy.[37] Nevertheless, actual toxicity studies would be required to make any conclusions about the safety of the tin porphyrin hydrogels.

Conclusion

In this work a pH-responsive hydrogel was generated by post chelating $SnCl_2$ into free base mTCPP hydrogels. This post chelation process was simple and effective. Tin porphyrin hydrogels provide a wide pH-responsive range and the potential for quantifying pH of the surrounding environment. The pH responsiveness was fully reversible in aqueous environments and in the presence of biomolecules found in serum. The tin porphyrin hydrogels, with extreme porphyrin density, were bright enough for facile transdermal fluorescence imaging following implantation and responded to changes in pH in vivo. Future work will aim to develop injectable hydrogels to avoid implantation surgery, to develop more quantitative ratiometric approaches and to assess toxicity. We conclude that tin porphyrin hydrogels hold potential for non-invasive, long term measurement of pH values inside the body.

Supplementary Material

Refer to Web version on PubMed Central for supplementary material.

Acknowledgements

This work was supported by the National Institutes of Health (DP5OD017898)

References

(1). Hoffman AS Hydrogels for biomedical applications. Adv Drug Deliv Rev 2012, 64, Supplement 18–23.

(2). Peppas NA; Van Blarcom DS Hydrogel-based biosensors and sensing devices for drug delivery. J Control Release 2016, 240 142–50. [PubMed: 26611939]

(3). Huang H; Song W; Chen G; Reynard JM; Ohulchanskyy TY; Prasad PN; Bright FV; Lovell JF Pd-Porphyrin-Cross-Linked Implantable Hydrogels with Oxygen-Responsive Phosphorescence. Adv Healthc Mater 2014, 3 (6), 891–6. [PubMed: 24259519]

(4). Zhang L; Su F; Buizer S; Lu H; Gao W; Tian Y; Meldrum D A dual sensor for real-time monitoring of glucose and oxygen. Biomaterials 2013, 34 (38), 9779–88. [PubMed: 24090834]

(5). Nichols SP; Koh A; Storm WL; Shin JH; Schoenfisch MH Biocompatible Materials for Continuous Glucose Monitoring Devices. Chem Rev 2013, 113 (4), 2528–49. [PubMed: 23387395]

(6). Heo YJ; Shibata H; Okitsu T; Kawanishi T; Takeuchi S Long-term in vivo glucose monitoring using fluorescent hydrogel fibers. Proc Natl Acad Sci USA 2011, 108 (33), 13399–403. [PubMed: 21808049]

(7). Shibata H; Heo YJ; Okitsu T; Matsunaga Y; Kawanishi T; Takeuchi S Injectable hydrogel microbeads for fluorescence-based in vivo continuous glucose monitoring. Proc Natl Acad Sci USA 2010, 107 (42), 17894–8. [PubMed: 20921374]

(8). Richter A; Paschew G; Klatt S; Lienig J; Arndt K-F; Adler H-J Review on Hydrogel-based pH Sensors and Microsensors. Sensors 2008, 8 (1), 561. [PubMed: 27879722]

(9). Wang H; Mao D; Wang Y; Wang K; Yi X; Kong D; Yang Z; Liu Q; Ding D Biocompatible fluorescent supramolecular nanofibrous hydrogel for long-term cell tracking and tumor imaging applications. Sci Rep 2015, 5 16680.

(10). Evans DF; Pye G; Bramley R; Clark AG; Dyson TJ; Hardcastle JD Measurement of gastrointestinal pH profiles in normal ambulant human subjects. Gut 1988, 29 (8), 1035–41. [PubMed: 3410329]

(11). Jin W; Jiang J; Wang X; Zhu X; Wang G; Song Y; Bai C Continuous intra-arterial blood pH monitoring in rabbits with acid–base disorders. Respir Physiol Neurobiol 2011, 177 (2), 183–8. [PubMed: 21402180]

(12). Grant SA; Bettencourt K; Krulevitch P; Hamilton J; Glass R In vitro and in vivo measurements of fiber optic and electrochemical sensors to monitor brain tissue pH. Sensor Actuat B: Chem 2001, 72 (2), 174–9.

(13). Georgiev NI; Bryaskova R; Tzoneva R; Ugrinova I; Detrembleur C; Miloshev S; Asiri AM; Qusti AH; Bojinov VB A novel pH sensitive water soluble fluorescent nanomicellar sensor for potential biomedical applications. Biorg Med Chem 2013, 21 (21), 6292–302.

(14). Davies TA; Fine RE; Johnson RJ; Levesque CA; Rathbun WH; Seetoo KF; Smith SJ; Strohmeier G; Volicer L; Delva L; Simons ER Non-age Related Differences in Thrombin Responses by Platelets from Male Patients with Advanced Alzheimer′s Disease. Biochem Biophys Res Commun 1993, 194 (1), 537–43. [PubMed: 8333868]

(15). Wencel D; Abel T; McDonagh C Optical Chemical pH Sensors. Anal Chem 2014, 86 (1), 15–29. [PubMed: 24180284]

(16). Schreml S; Meier RJ; Weiß KT; Cattani J; Flittner D; Gehmert S; Wolfbeis OS; Landthaler M; Babilas P A sprayable luminescent pH sensor and its use for wound imaging in vivo. Exp Dermatol 2012, 21 (12), 951–3. [PubMed: 23171458]

(17). Lee MH; Han JH; Lee JH; Park N; Kumar R; Kang C; Kim JS Two-Color Probe to Monitor a Wide Range of pH Values in Cells. Angew Chem Int Ed 2013, 52 (24), 6206–9.

(18). Yang Z; Qin W; Lam JWY; Chen S; Sung HHY; Williams ID; Tang BZ Fluorescent pH sensor constructed from a heteroatom-containing luminogen with tunable AIE and ICT characteristics. Chem Sci 2013, 4 (9), 3725–30.

(19). Shi W; Li X; Ma H A Tunable Ratiometric pH Sensor Based on Carbon Nanodots for the Quantitative Measurement of the Intracellular pH of Whole Cells. Angew Chem Int Ed 2012, 124 (26), 6538–41.

(20). Ni Y; Wu J Far-red and near infrared BODIPY dyes: synthesis and applications for fluorescent pH probes and bio-imaging. Org Biomol Chem 2014, 12 (23), 3774–91. [PubMed: 24781214]

(21). Qu F; Li NB; Luo HQ Highly Sensitive Fluorescent and Colorimetric pH Sensor Based on Polyethylenimine-Capped Silver Nanoclusters. Langmuir 2013, 29 (4), 1199–205. [PubMed: 23282222]

(22). Huang H; Song W; Rieffel J; Lovell JF Emerging applications of porphyrins in photomedicine. Front Phys 2015, 3 (23).

(23). Zhang Y; Lovell JF Porphyrins as Theranostic Agents from Prehistoric to Modern Times. Theranostics 2012, 2 (9), 905–15. [PubMed: 23082102]

(24). Huang H; Lovell JF Advanced Functional Nanomaterials for Theranostics. Adv Funct Mater 2017,27 (2), 1603524. [PubMed: 28824357]

(25). Zhang Y; Lovell JF Recent applications of phthalocyanines and naphthalocyanines for imaging and therapy. WIRES: Nanomed Nanobiotechnol 2017, 9 (1), e1420.

(26). Huang H; Wang D; Zhang Y; Zhou Y; Geng J; Chitgupi U; Cook TR; Xia J; Lovell JF Axial PEGylation of Tin Octabutoxy Naphthalocyanine Extends Blood Circulation for Photoacoustic Vascular Imaging. Bioconjugate Chem 2016, 27 (7), 1574–8.

(27). Huang H; Hernandez R; Geng J; Sun H; Song W; Chen F; Graves SA; Nickles RJ; Cheng C; Cai W; Lovell JF A porphyrin-PEG polymer with rapid renal clearance. Biomaterials 2016, 76 25–32. [PubMed: 26517562]

(28). Lovell JF; Roxin A; Ng KK; Qi Q; McMullen JD; DaCosta RS; Zheng G Porphyrin-Cross-Linked Hydrogel for Fluorescence-Guided Monitoring and Surgical Resection. Biomacromolecules 2011, 12 (9), 3115–8. [PubMed: 21777008]

(29). Grigg R; Norbert WDJA The proton-controlled fluorescence of aminomethyltetraphenylporphyrin-tin(IV) derivatives. J Chem Soc Chem Commun 1992, (18), 1298–300.

(30). Chaniotakis NA; Park SB; Meyerhoff ME Salicylate-selective membrane electrode based on tin(IV)-tetraphenylporphyrin. Anal Chem 1989, 61 (6), 566–70. [PubMed: 2729591]

(31). George RC; Egharevba GO; Nyokong T Spectroscopic studies of nanostructures of negatively charged free base porphyrin and positively charged tin porphyrins. Polyhedron 2010, 29 (5), 1469–74.

(32). Delmarre D; Veret-Lemarinier A-V; Bied-Charreton C Spectroscopic properties of Sn(IV) tetrapyridyl and tetramethylpyridinium porphyrins in solution and in sol–gel matrices. J Lumin 1999, 82 (1), 57–67.

(33). Manke A-M; Geisel K; Fetzer A; Kurz P A water-soluble tin(iv) porphyrin as a bioinspired photosensitiser for light-driven proton-reduction. PCCP 2014, 16 (24), 12029–42. [PubMed: 24556846]

(34). Schreml S; Szeimies RM; Karrer S; Heinlin J; Landthaler M; Babilas P The impact of the pH value on skin integrity and cutaneous wound healing. J Eur Acad Dermatol Venereol 2010, 24 (4), 373–8. [PubMed: 19703098]

(35). Schreml S; Meier RJ; Kirschbaum M; Kong SC; Gehmert S; Felthaus O; Küchler S; Sharpe JR; Wöltje K; Weiß KT Luminescent dual sensors reveal extracellular pH-gradients and hypoxia on chronic wounds that disrupt epidermal repair. Theranostics 2014, 4 (7), 721–35. [PubMed: 24883122]

(36). Rüdel H Case study: bioavailability of tin and tin compounds. Ecotoxicol Environ Safety 2003, 56 (1), 180–9. [PubMed: 12915151]

(37). Josefsen LB; Boyle RW Photodynamic Therapy and the Development of Metal-Based Photosensitisers. Met Based Drugs 2008, 2008 276109.

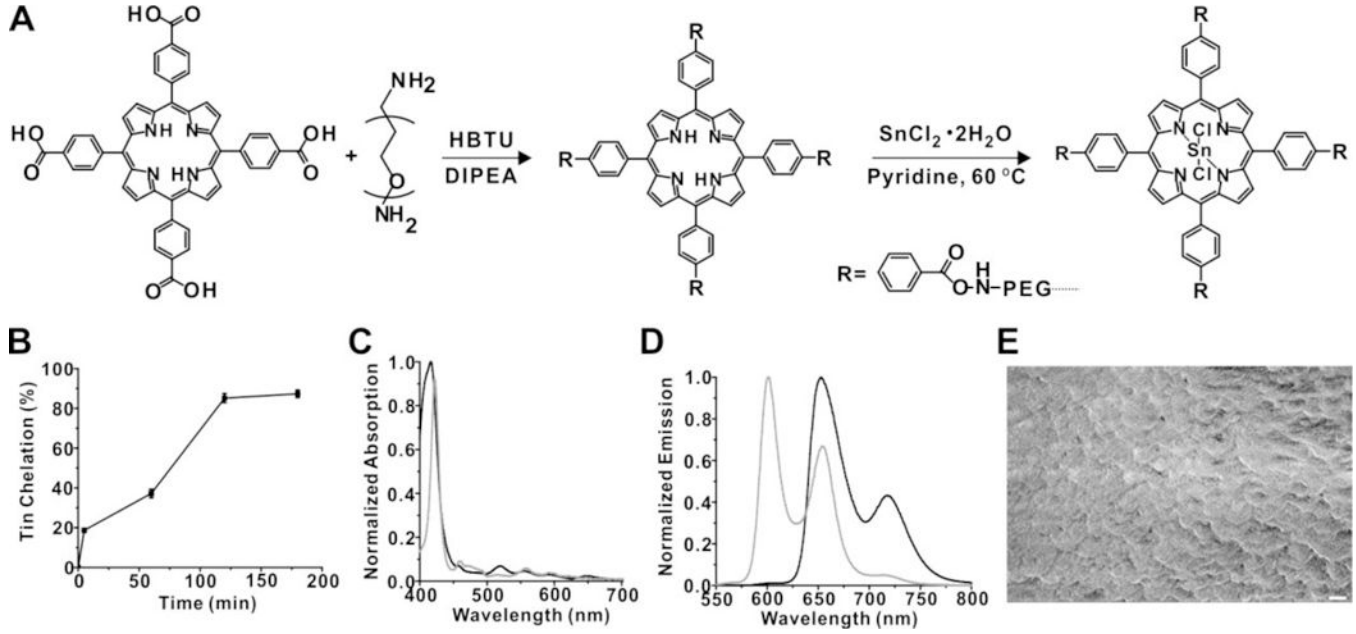

Figure 1. Synthesis of tin-porphyrin-PEG hydrogels.

A) Synthesis of 2H mTCPP hydrogel and subsequent tin chelation. **B)** Kinetics of $SnCl_2$ chelation. Data show mean +/− std. dev. for n=3 separate chelation reactions. **C)** Absorbance and **D)** fluorescence spectra of 2H-mTCPP (black) and $SnCl_2$mTCPP (grey) hydrogels. **E)** Scanning electron micrograph of a freeze-dried portion of $SnCl_2$mTCPP hydrogel. 1 μm scale bar is shown.

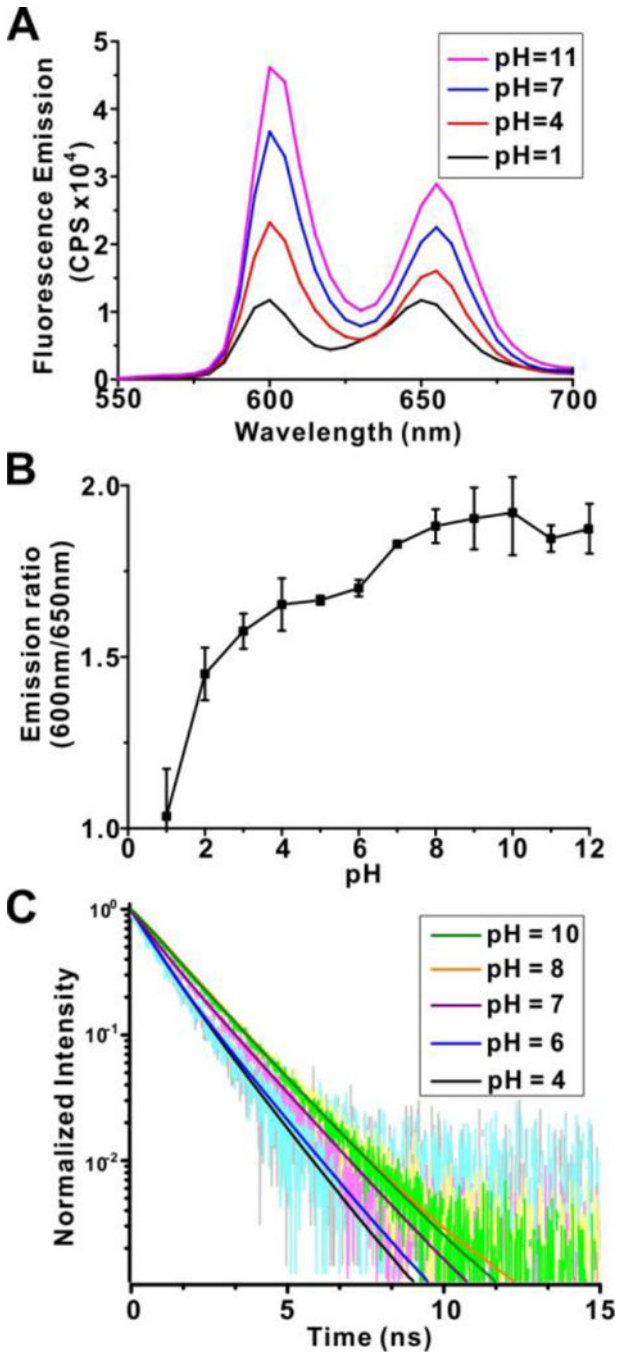

Figure 2. pH sensitivity of tin-porphyrin-PEG hydrogels.

A) Fluorescence spectra of $SnCl_2$mTCPP hydrogels in pH=1–12 100 mM sodium phosphate solutions. **B)** Ratio of $SnCl_2$mTCPP hydrogel fluorescence emission intensities at 600 nm and 650 nm. Data show mean +/− std. dev. for n=3 separate polymerization reactions and purifications. **C)** Fluorescence lifetime at 600 nm emission of $SnCl_2$mTCPP hydrogels in 100 mM sodium phosphate at indicated pH.

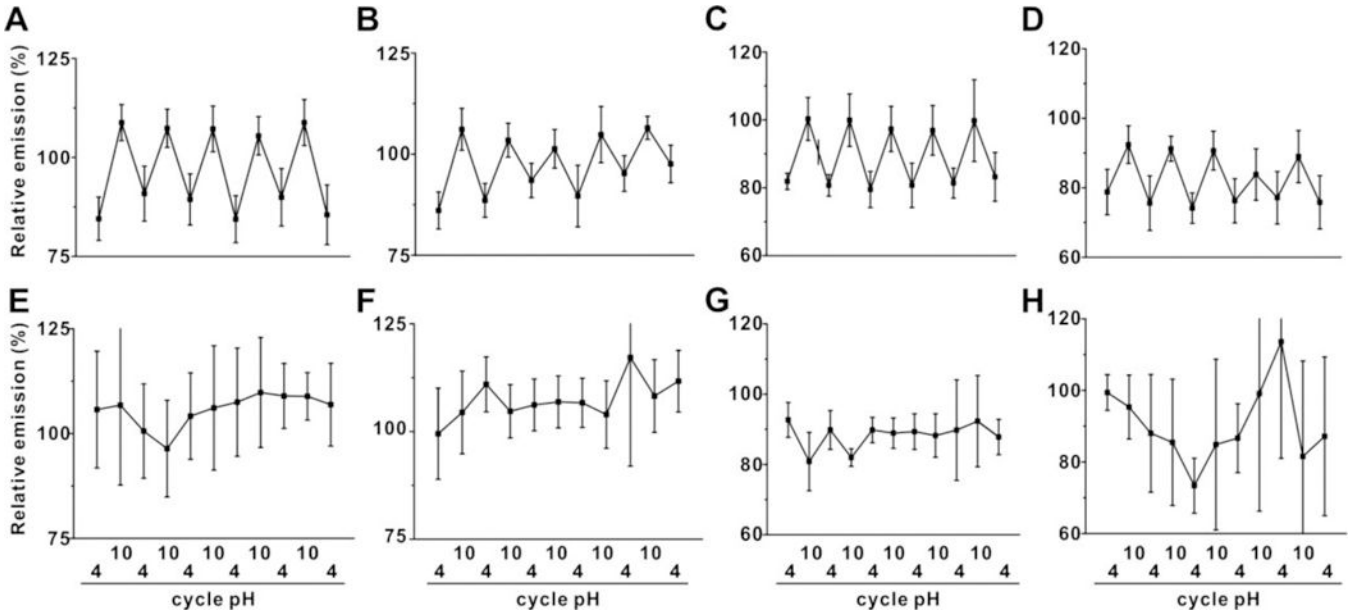

Figure 3. pH-responsive fluorescence reversibility of tin or free base porphyrin hydrogels.

Fluorescence emission (normalized to initial emission after formation) of tin porphyrin-PEG hydrogels (top row) or freebase porphyrin-PEG hydrogels (bottom row) placed in 100 mM sodium phosphate solutions of indicated pH (**A**; **E**) and after one week of storage (**B**; **F**). Emission in the presence of 10% fetal bovine serum (FBS) (**C; G**). and after one week of storage in FBS (**D** and **H**). Data show mean +/− std. dev. for n=3 separate polymerization reactions.

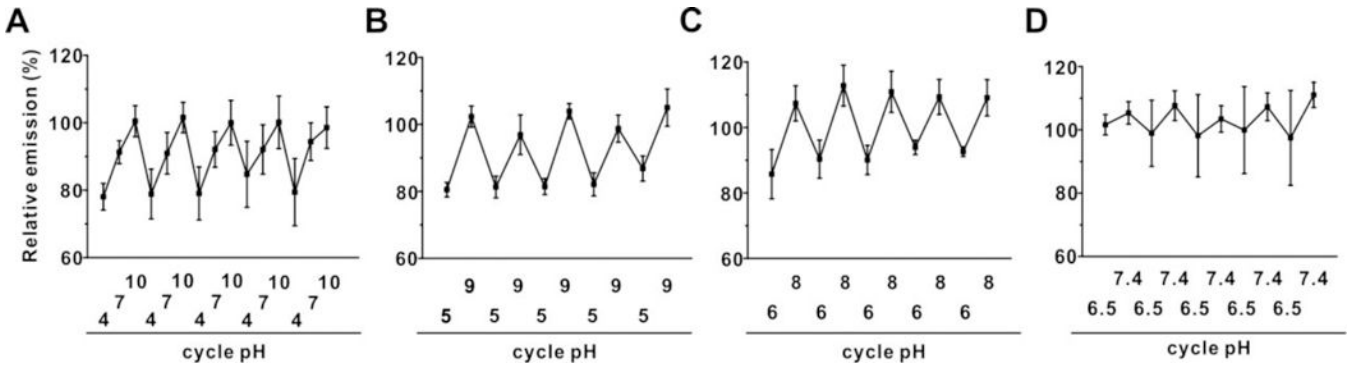

Figure 4. Sensitivity towards intermediate pH by tin-porphyrin-PEG hydrogels.

Fluorescence emission (normalized to initial emission after formation) of tin porphyrin-PEG hydrogels placed in 100 mM sodium phosphate solutions of **A)** pH=4, 7, and 10. **B)** pH=5 and 9, and **C)** pH=6 and 8. **D)** Fluorescence emission (normalized to initial emission after formation) of tin porphyrin-PEG hydrogels placed in pH=6.5 and 7.4 PBS buffer. Data show mean +/− std. dev. for n=3 separate polymerization reactions.

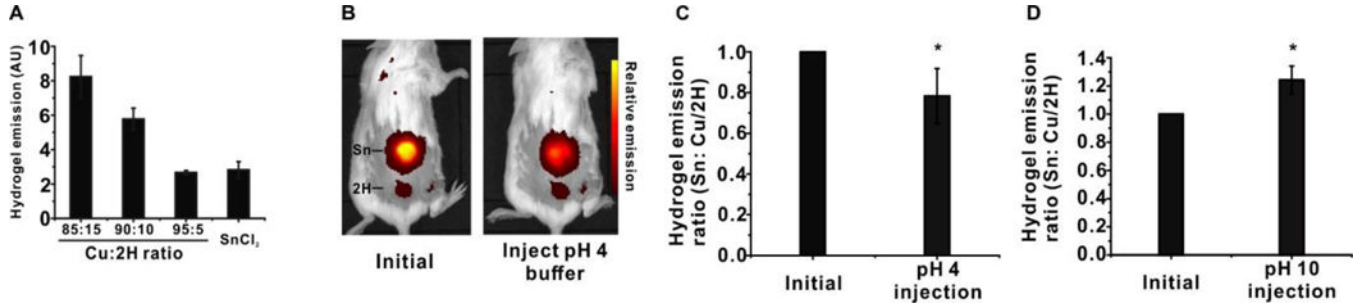

Figure 5. Hydrogel implantation for non-invasive pH sensing in vivo.

A) Fluorescence emission of Cu:2H blended porphyrin hydrogels (non pH-responsive) relative to tin ones (pH-responsive). **B)** Fluorescent images of living mice with an implanted tin hydrogel (top) and Cu:2H hydrogel (bottom), pre- and post- subcutaneous injection with pH=4 100 mM sodium phosphate. Relative transdermal fluorescence emission ratios of tin and Cu:2H hydrogels in mice implanted with hydrogels before and after injection with **C)** pH=4 and **D)** pH=10 phosphate solutions. Data show mean +/− std. dev. for n=3 separate mice, * indicates a statistically significant change based on a two-tailed student's t-test ($p<0.01$).